Stochastic 16-State Model of Voltage Gating of Gap-Junction Channels Enclosing Fast and Slow Gates

Nerijus Paulauskas,[†¶] Henrikas Pranevicius,[‡] Jonas Mockus,[§] and Feliksas F. Bukauskas[†]

[†]Dominick P. Purpura Department of Neuroscience, Albert Einstein College of Medicine, New York, New York; [‡]Department of Business Informatics, Kaunas University of Technology, Kaunus, Lithuania; [§]Department of Systems Analysis, Institute of Mathematics and Informatics, Vilnius University, Vilnius, Lithuania; and [¶]Institute of Cardiology, Lithuanian University of Health Sciences, Kaunas, Lithuania

Supporting Material

Figures S1-S3:

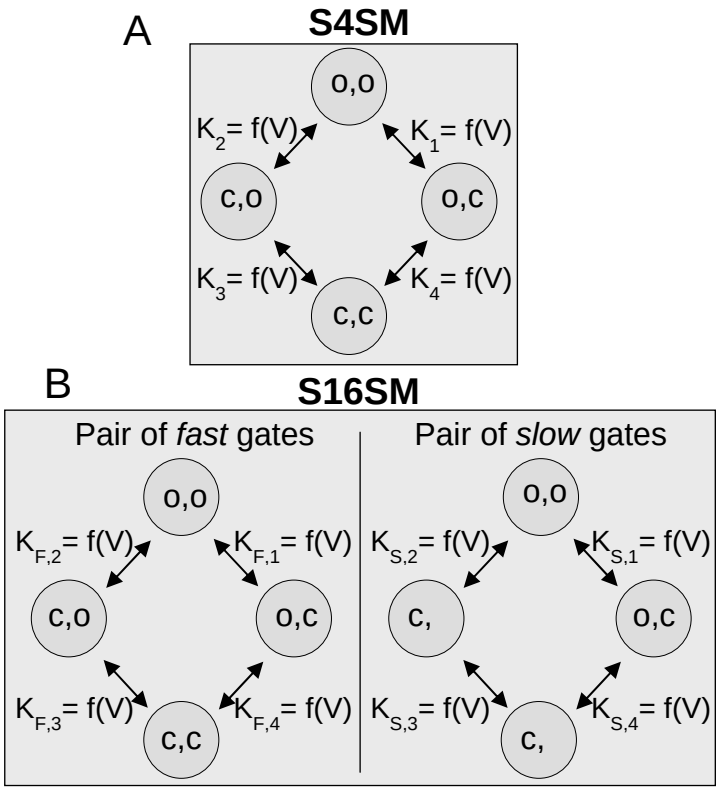

Fig. S1. Schematics of the channel states in four- (**A**) and 16- (**B**) state voltage-gating models of GJs.

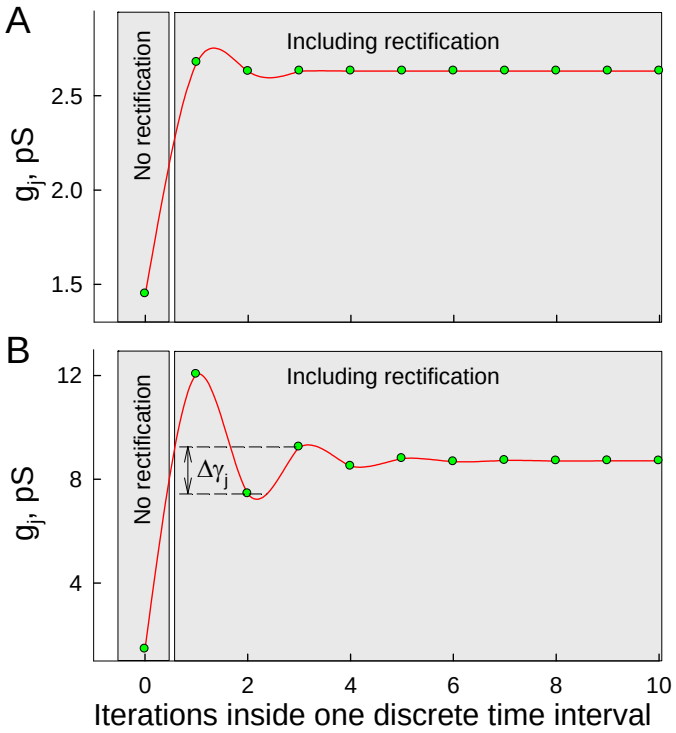

Fig. S2. Dependence of the single GJ channel conductance, γ_j, on the number of iterations used to evaluate an effect of I/V rectification on $\gamma_{F,open}$, $\gamma_{F,res}$ and $\gamma_{S,open}$ in a simulated Cx45 GJ channel (Table S3). Iterations were performed inside a discrete time interval. (**A**) Initially, one *fast* gate was closed ($\gamma_{F,res}$=1.5 pS) while

both *slow* gates and one *fast* gate were open ($\gamma_{F,open}$ = $\gamma_{S,open}$=128 pS) and the GJ channel was exposed to V_j=100 mV. Rectification coefficients were as follows: $R_{F,res}$=150 mV, $R_{F,open}$= $R_{S,open}$=1000 mV. In the first step, voltages were calculated across each gate (V_Gs) assuming an absence of I/V rectification. Then, using these voltages, gate conductances were recalculated accounting for their rectification to evaluate a new set of V_Gs. We repeated this cycle 10 times, and evaluated γ_j as well as differences, $\Delta\gamma_{j,n}=\gamma_{j,n+1}-\gamma_{j,n}$, in each cycle. (**B)** All parameters were the same as in (**A**), except $R_{F,res}$=40 mV, which is too low and practically never occurs. Given examples illustrate that the steady state of γ_j was approached after approximately 4 cycles in (**A**) and 7 cycles in (**B**). In a S16SM, to avoid an infinite loop, we defined the tolerance criterion $e=\gamma_{j,o}/10{,}000$ and, at $\Delta\gamma_j<e$, the final values of V_Gs were estimated, allowing for the evaluation of possible changes in the state of each gate. Finally, the information about the new set of states for all gates is transferred to the next discrete time interval and the process iteratively repeated.

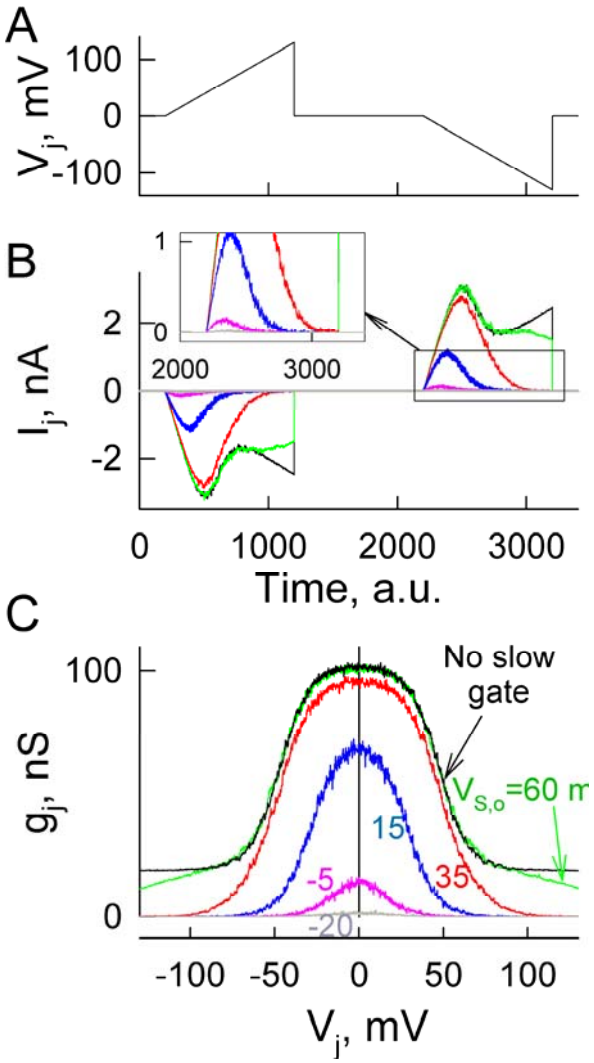

Fig. S3. Illustrates how an addition of the *slow* gate to an already present *fast* gate affects g_j-V_j plots obtained using slow V_j ramps (**A**). Simulated junction containing 1000 channels. Values of parameters are shown in Table S1. I_j and g_j traces in different colors were obtained at $V_{S,o}$ equal to 60, 35, 15, -5 and -20 mV; I_j trace (**B**) and g_j-V_j plot shown in black (**C**) were obtained when the operation of the *slow* gate was fully inactivated. Presented data show that a gradual reduction in $V_{S,o}$ decreases g_{min} to zero, narrows g_j-V_j plot and finally leads to full uncoupling at $V_{S,o}$s below -20 mV. Thus, the presented example shows that an increase in sensitivity to V_j of the *slow* gate can reduce g_{min} and lead to full uncoupling even at constant parameters of the fast gate. In the a S4SM, containing only two fast gates, a decay of g_{min} can be caused only by reducing $\gamma_{F,res}$.

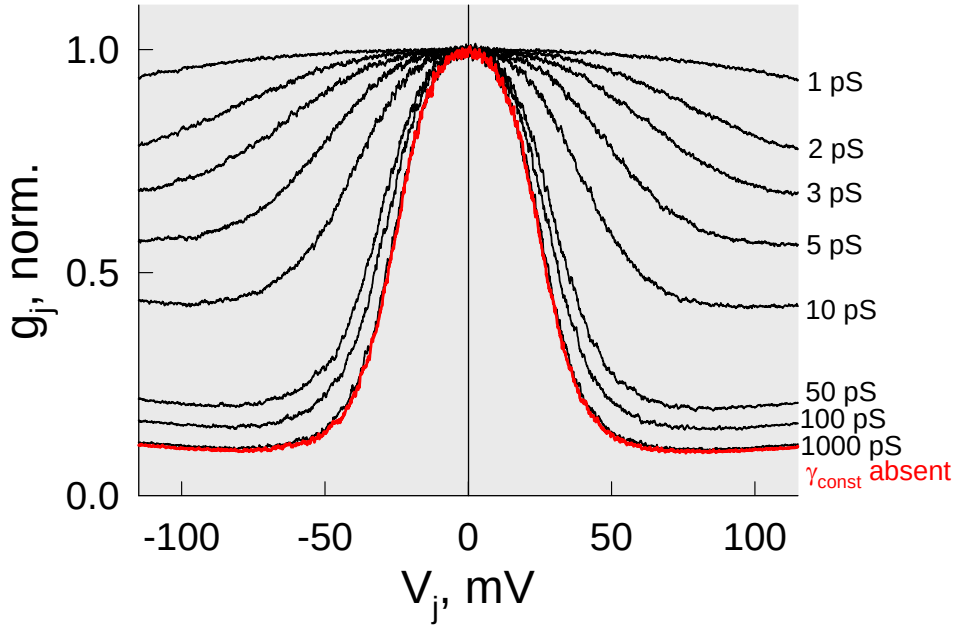

Fig. S4. A family of simulated and normalized g_j-V_j plots obtained using a S16SM and parameters of Cx45 homotypic GJs shown in **Table S3**; 5000 GJ channels were operating. In the absence of non-gated conductance ($\gamma_{const} \rightarrow \infty$), the g_j-V_j plot is in red. Under a decrease of γ_{const} from 1000 to 1 pS, g_j-V_j plots become less sensitive to V_j. Together, g_{min} increases, which is due to relatively greater decrease of γ_{open} than γ_{res} of the GJ channel.

Tables S1-S5:

Table S1. Parameters of *fast* and *slow* gates used to simulate voltage-gating shown in Figs. 2.

Parameters of gates	***Fast* gate**	***Slow* gate**
A_F & A_s, mV^{-1}	0.11	0.09
$V_{F,o}$ & $V_{S,o}$, mV	25	60
$\gamma_{F,open}$ & $\gamma_{S,open}$, pS	440	440
$R_{F,open}$ & $R_{S,open}$ mV	800	800
$\gamma_{F,res}$ & $\gamma_{S,closed}$, pS	25.9	-
$R_{F,res}$ & $R_{S,closed}$, mV	300	-

Table S2. Initial range of variable parameters used to fit g_j-V_j plot of Cx45 homotypic GJs shown in Fig. 5A and their preliminary/initial estimates.

Parameters of gates	***Fast* gate; initial range of parameters**	***Slow* gate; initial range of parameters**	***Fast* gate; initial estimates**	***Slow* gate; initial estimates**
A_F & A_s, mV^{-1}	0.08 ÷ 0.14	0.06 ÷ 0.12	0.14	0.109
$V_{F,o}$ & $V_{S,o}$, mV	-20 ÷ 40	40 ÷ 100	12.9	88
$\gamma_{F,open}$ & $\gamma_{S,open}$, pS	128	128	128	128
$R_{F,open}$ & $R_{S,open}$ mV	1000	1000	1000	1000
$\gamma_{F,res}$ & $\gamma_{S,closed}$, pS	1 ÷ 10	0	1.36	0
$R_{F,res}$ & $R_{S,closed}$, mV	100 ÷ 300	-	159	-

Table S3. The final estimates of gating parameters of Cx45 GJs from g_j-V_j plot shown in Fig. 5A.

Parameters of gates	***Fast* gate, hemich. A**	***Slow* gate, hemich. A**	***Fast* gate, hemich. B**	***Slow* gate, hemich. B**
A_F & A_s, mV^{-1}	0.14	0.11	0.15	0.11
$V_{F,o}$ & $V_{S,o}$, mV	13.4	88	13.7	84.9
$\gamma_{F,open}$ & $\gamma_{S,open}$, pS	128	128	128	128
$R_{F,open}$ & $R_{S,open}$ mV	1000	1000	1000	1000
$\gamma_{F,res}$ & $\gamma_{S,closed}$, pS	1.5	0	1.49	0
$R_{F,res}$ & $R_{S,closed}$, mV	151	-	140	-

Table S4. The estimates of gating parameters of Cx43-EGFP/Cx45 GJs obtained from global optimization of experimental g_j-V_j plot shown in Fig. 5C.

Parameters of gates	***Fast* gate Cx45**	***Slow* gate Cx45**	***Fast* gate Cx43-EGFP**	***Slow* gate Cx43-EGFP**
A_F & A_s, mV^{-1}	0.16	0.18	0.1	0.067
$V_{F,o}$ & $V_{S,o}$, mV	2.1	61	40	48.7
$\gamma_{F,open}$ & $\gamma_{S,open}$, pS	128	128	440	440
$R_{F,open}$ & $R_{S,open}$ mV	1000	1000	1000	1000
$\gamma_{F,res}$ & $\gamma_{S,closed}$, pS	0.42	0	440	0
$R_{F,res}$ & $R_{S,closed}$, mV	109.8	-	-	-

Table S5. Gating parameters used for simulation of $g_{j,ss}$-V_j plots shown in Fig. S3.

Parameters	***Fast* gate**	***Slow* gate**
A_F & A_s,, mV^{-1}	0.1	0.06
$V_{F,o}$ & $V_{S,o}$, mV	20	60, 35, 15, -5 or -20
$\gamma_{F,open}$ & $\gamma_{S,open}$, pS	400	400
$R_{F,open}$ & $R_{S,open}$ mV	1000	1000
$\gamma_{F,res}$ & $\gamma_{S,closed}$, pS	23	0
$R_{F,res}$ & $R_{S,closed}$, mV	1000	-

Legends to Movies 1-3.

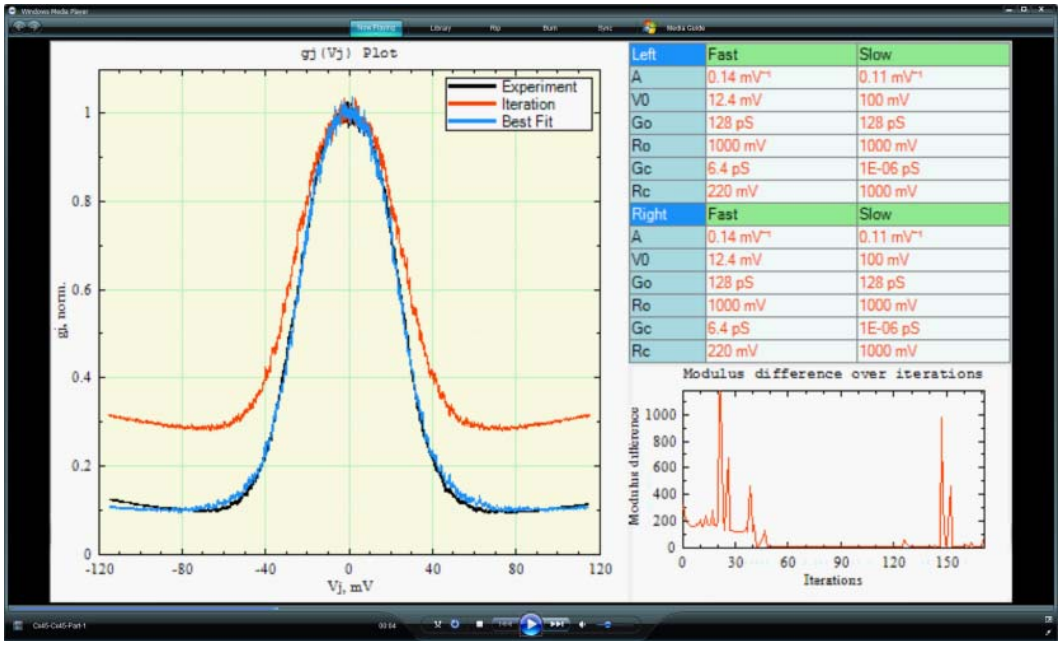

Movie 1. Illustration of coarse global optimization of gating parameters of Cx45 homotypic gap junction channels from experimental $g_{j,ss}$-V_j dependence (black) assuming that parameters of *fast* and *slow* gates in both hemichannels are identical. **A single frame** from the movie is shown above. Simulated $g_{j,ss}$-V_j plots are shown in red. The $g_{j,ss}$-V_j plot (blue) shows intermediate best fits that gradually approach the experimental $g_{j,ss}$-V_j plot (black). The table and numbers on the right show changes of individual parameters during global optimization. The plot on the bottom-right shows the dynamics of modulus difference between simulated and experimental $g_{j,ss}$-V_j plots during global optimization.

Movie 2. Illustration of 'final' global optimization of gating parameters of Cx45 homotypic gap junction channels from experimental $g_{j,ss}$-V_j dependence (black) assuming that parameters of *fast* and *slow* gates in both hemichannels differ. Simulated $g_{j,ss}$-V_j plots (red) and comprise 950 iterations. The $g_{j,ss}$-V_j plot (blue) shows intermediate best fits that gradually approach the final $g_{j,ss}$-V_j plot. The 'final' global optimization starts with gating parameters obtained during the 'coarse' global optimization. The table and numbers on the right show changes of individual parameters during global optimization. The plot on the bottom-right shows dynamics of modulus difference between simulated and experimental $g_{j,ss}$-V_j plots during global optimization.

Movie 3. Illustration of global optimization of gating parameters of Cx43-EGFP/Cx45 heterotypic gap junction channels from experimental $g_{j,ss}$-V_j dependence (black) assuming that parameters of *fast* and *slow* gates in both hemichannels differ. Simulated $g_{j,ss}$-V_j plots (red) comprise 1680 iterations. The $g_{j,ss}$-V_j plot (blue) shows intermediate best fits that gradually approach the final $g_{j,ss}$-V_j plot. The table and numbers on the right show changes of individual parameters during global optimization. The plot on the bottom-right shows dynamics of modulus difference between simulated and experimental $g_{j,ss}$-V_j plots during global optimization.